11 Phase transitions and superconducting photon detectors

M. Reibelt, R. Dell'Amore, H. Bartolf, S. Siegrist, L. Gómez, A. Engel and A. Schilling

in collaboration with: Paul Scherrer Institute, University of Bern (K. Krämer), EPF Lausanne (H. Berger), Bhaba Atomic Research Center (G. Ravikumar), Forschungszentrum Karlsruhe (Th. Wolf, H. Küpfer), Universität Karlsruhe (K. Il'in), ETH Zürich (J. Karpinksi), Deutsches Zentrum für Luft- und Raumfahrt (H.-W. Hübers), University of Wellington (B. Ruck), Istituto Nazionale di Ricerca Metrologica I.N.RI.M Torino (C. Portesi), FIRST Lab ETH Zürich.

11.1 Physics of superconducting thin-film nanostructures and possible applications as fast single-photon detectors

Superconducting single-photon detectors (SSPD) which are based on a current-biased superconducting meander strip, have been attracting a lot of attention. They are extremely fast and very sensitive and could be used in such diverse areas as quantum encryption, infrared astronomy or spectroscopy. We are working on a better understanding of the detection principle and to shed a light on the underlying physics of superconducting nanostructures.

E-beam lithography

The performance of SSPD crucially depends on the quality of the lithographic processes during their production. The strip cross-section and the parameters characterizing the superconducting state have to be as homogeneous as possible along the entire length of the strip. Therefore, we are continuously working on improving our lithographic technologies. During the last year we have implemented a dry-etching step into our production process.

Our collaborating partners at the University of Karlsruhe produce high-quality NbN films with thickness typically between 4 and 10 nm. These films are prepared by DC-magnetron sputtering. In order to achieve homogeneous films with a high T_c the sapphire substrate needs to be heated to about 750°C. These high temperatures during film deposition prohibit the use of the lift-off technique. Our alternative approach starts from such extended films. Using e-beam lithography we then write the desired structure into a resist that is put on top of the NbN film. Reactive ion etching is then used to remove the unprotected areas of the NbN film.

After additional photolithography processes to make the necessary conduction paths for connecting the device to external electronics we obtain the final structures. In Fig. 11.1 we show an example of a meander structure with 200 nm wide and 10 nm thin strips. This

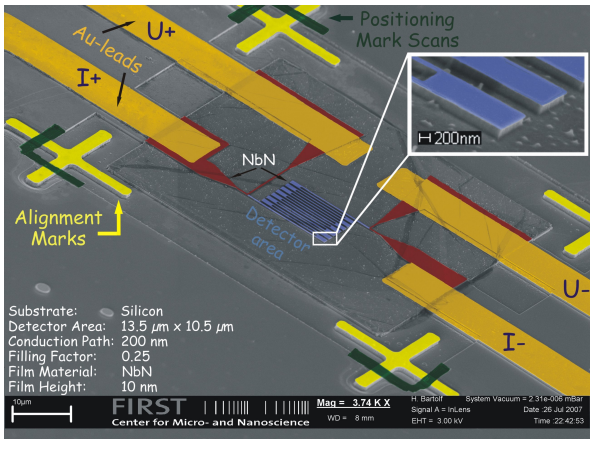

Figure 11.1: SEM picture of a 200 nm wide NbN meander on a Si substrate in false color representation to emphasize different elements.

meander showed excellent superconducting properties (1). Similar structures will be tested to demonstrate their potential as SSPD.

Critical-current density in NbN bridges

The detection model that has been previously described in detail requires bias currents of about 90% to 95% of the depairing critical-current density. Such high current densities can only be reached if the meander strip lines remain free of magnetic vortices, otherwise the dissipation-free current transport will be limited by the depinning of vortices. We have systematically measured critical-current densities in NbN bridges with widths ranging from 100 nm to 10 μm to shed light on the mechanism determining the critical-current density.

We have found that the experimentally determined critical-current densities in sub-μm wide bridges can be well described by the mean-field *Ginzburg-Landau* depairing critical current density (see Fig. 11.2 for a 300 nm wide bridge). Wider bridges deviate substantially from this temperature-dependence below a certain temperature. We interpret this reduction in critical-current density below the expectations for the depairing critical-current density as the entry of vortices due to self-field of the applied current. This can be qualitatively described with an edge-barrier model (2) taking into account edge effects in analogy to the *Bean-Livingston* surface barrier (3).

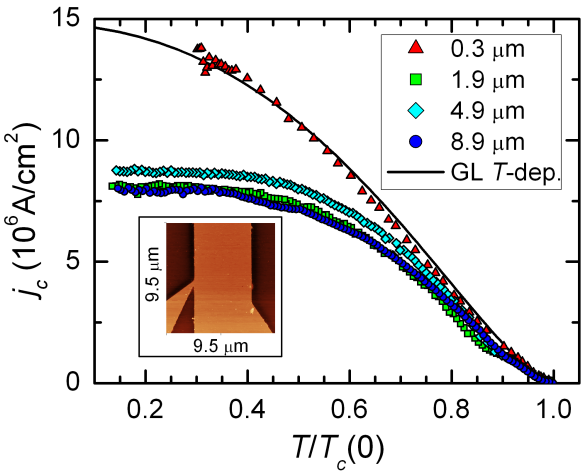

Figure 11.2: Critical current density j_c as a function of reduced temperature $T/T_c(0)$ for NbN bridges of different widths. The solid line is a fit of the Ginzburg-Landau depairing critical-current density to the data of the 300 nm wide bridge. The inset shows an AFM-image of the 4.9 μm wide bridge.

Transition metal nitrides

Currently, NbN is used as the standard material for these kind of single-photon detectors and in many respects it is a very good material. However, to increase the spectral range of these detectors and to check the validity of the detection model, the use of other superconducting materials would also be interesting. In 2007 a versatile magnetron sputtering machine has been installed in the FIRST lab at ETHZ. This has opened up the opportunity to prepare a whole range of elemental and composite superconducting thin films. We have already been able to prepare amorphous MoN films with $T_c \approx 6$ K. We will further optimize deposition parameters and characterize these films to evaluate their potential as an alternative to NbN.

11.2 Low temperature magnetic field dependence of the specific heats of V_3Si and $LuNi_2B_2C$

The differential-thermal analysis (DTA) method used in our laboratory is particularly suited to detect sharp phase transitions, e.g., first-order phase transitions, and it does not require large sample masses (4; 5). Since very high quality samples often only exist in form of small crystals, such a sensitive method is of high value. In addition, it is often desirable to choose a method that yields a high data-point density

within a reasonable measuring time. Common techniques, such as AC or relaxation methods, are sensitive but very time consuming. As an example, the relaxation method implemented in a commercial PPMS platform (Quantum Design) usually takes several *minutes* per data point for data acquisition while the DTA technique takes only approximately 3 *seconds* per data point, at an impressive data-point density of typically 170 data points per Kelvin. High resolution and high data-point density are needed for the observation of small and sharp effects.

In superconductors, not only the discontinuity in the specific heat at T_c contains valuable information about the superconducting state, but also the field dependence of this quantity below T_c is of utmost interest because it may be influenced by the symmetry of the order-parameter and perhaps also by other factors (6; 7; 8; 9).

V_3Si

In the standard theory of superconductivity the magnetic-field dependence of the specific heat in the mixed state is $\Delta c_p/T(H) = (c_p(H) - c_p(H=0))/T = \gamma H/H_{c2}(T)$ for $T \to 0$, where γ is the Sommerfeld coefficient characterizing the specific heat of the electronic system in the normal sate. In this classic scenario, $\gamma(H)$, a thermodynamic probe of the electronic density of states at low energy, is expected to be linear in H up to H_{c2} (10). At temperatures $T > 0$, the field dependence of $\Delta c_p/T$ is expected to be more complicated, and a non-linear behavior has been observed in a number of compounds.

We measured the specific heat of V_3Si for fields up to H=8.3 T. Fig. 11.3 shows two DTA data sets for $\mu_0 H = 0$ T and 6 T. The $\mu_0 H = 6$ T data show a structural martensitic transition taking place close to T_{c0}, which is nearly entirely suppressed by superconductivity in zero magnetic field. Figure 11.4 shows a small temperature interval around T=7.5 K for selected fields. The non-linear field dependence at low magnetic fields is already visible in this figure.

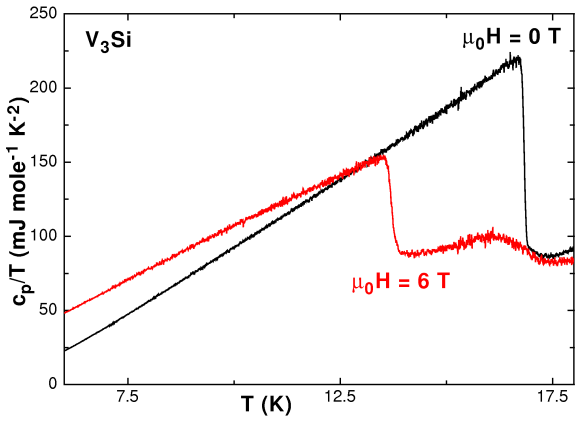

Figure 11.3: c_p/T-DTA data of a V_3Si single crystal for $\mu_0 H$=0 T and 6 T.

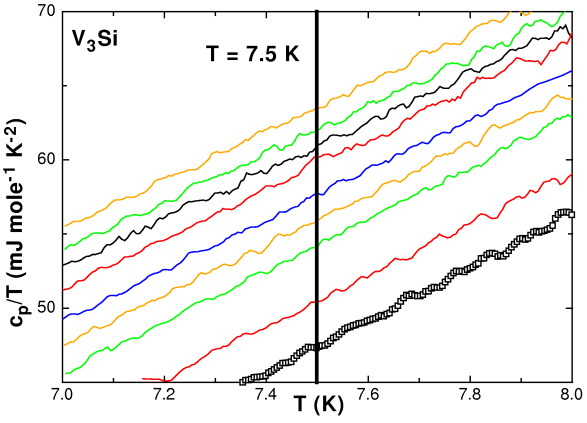

Figure 11.4: c_p/T-DTA data of V_3Si in a small temperature interval around T=7.5 K, starting with $\mu_0 H$=0 T (open circles) for the lowest curve and 4 T for the highest curve, $\mu_0 H$ increasing in intervals of 0.5 T.

Extracting the $c_p/T(H)$ data for a fixed temperature T=7.5 K results in the data plotted in Fig. 11.5(a), demonstrating the magnetic-field dependent specific-heat difference $\Delta c_p/T(H)$ of V_3Si (open circles). The dashed line is a guide to the eye and visualizes an approximately linear behavior above $\mu_0 H > 2$ T. It can clearly be seen that the data deviate from linearity below $\mu_0 H < 2$ T

where it is better described by a $H^{1/2}$ dependence. For comparison, we have plotted in the same figure the data of Ramirez (11) from a polycrystalline V_3Si sample. The deviation from linearity becomes very significant for low fields close to the lower critical field H_{c1}. In analogy to Ref. (11) we can fit our data to $\Delta c_p/T = A(H - H^*_{c1})^{1/2}$ with $H^*_{c1} = 0.2$ T being the field where magnetic flux starts to enter the sample, and $A \approx 8.6$ mJ mole^{-1} K^{-2} T$^{-1/2}$, in good agreement with the result of Ref. (11).

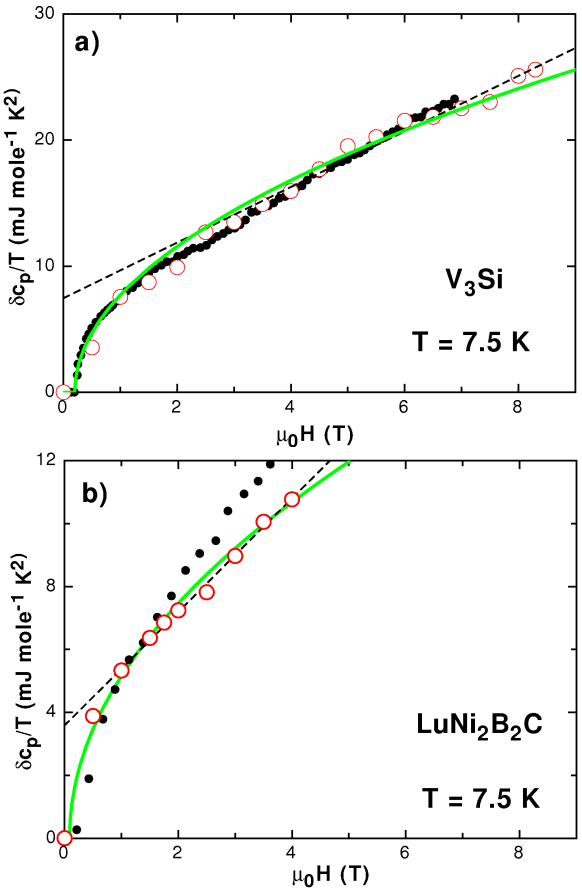

Figure 11.5: Magnetic-field dependence of the specific heat difference Δc_p/T at T=7.5 K for different crystals. The thick lines represent fits according to Δc_p/T=A(H-H^{1*}_{c1})$^{1/2}$ (see text). The dashed lines are guides to the eye to visualize the approximate linear behavior for the magnetic fields $\mu_0 H > 2$ T in the case of V_3Si and $\mu_0 H > 1$ T in the case of $LuNi_2B_2C$.
(a): data of a V_3Si single crystal obtained from DTA measurements (open circles), in comparison with the data of Ramirez [11](filled circles).
(b): data of a $LuNi_2B_2C$ single crystal obtained from DTA measurements (open circles), together with the data of Nohara et al. [12] (filled circles).

$LuNi_2B_2C$

Figure 11.5(b) shows in a similar way the magnetic field dependent $\Delta c_p/T$-DTA data for a $LuNi_2B_2C$ single crystal, obtained at a fixed temperature T=7.5 K. The dashed line is a guide to the eye and visualizes the linear behavior above $\mu_0 H > 1$T. Again it can clearly be seen that the data deviate from linearity below $\mu_0 H < 1$T where it is better described by a $H^{1/2}$ dependence. A fit according to $\Delta c_p/T = A(H - H_{c1})^{1/2}$ with $H_{c1} = 87$ mT ((13)) gives $A \approx 5.4$ mJ mole^{-1} K^{-2}T$^{-1/2}$.

For comparison we have reproduced the data of Nohara *et al.* (12) for $LuNi_2B_2C$ in Fig. 11.5. Again, our data confirm the observation that also in $LuNi_2B_2C$ $\Delta c_p/T$ is not linear in H.

These findings are noteworthy since both V_3Si and $LuNi_2B_2C$ are supposed to be s-wave systems. While the deviation of $\Delta c_p(H)/T$ from linearity and especially its approximate $\propto H^{1/2}$ dependence is usually interpreted as an indication for lines of nodes in the energy gap (8), one can state here that such a behavior as we observe in the s-wave superconductors V_3Si and $LuNi_2B_2C$ is likely a more a general phenomenon of type II superconductors.

11.3 Bose-Einstein condensation in $TlCuCl_3$?

$TlCuCl_3$ is a quantum- spin- $\frac{1}{2}$ system, that shows a gap between the ground state and

the first excited states for low magnetic fields $\mu_0 H_c \lessapprox 5.5\mathrm{T}$ and at low temperatures. At higher magnetic fields the gap is suppressed, and a Bose-Einstein condensation (BEC) of magnetic S=1 excitations (called triplons or magnons) is supposed to occur, leading to a magnetic phase with anti-ferromagnetic long-range order of the transverse spin components.

Meanwhile a considerable number of other materials have been found that exhibit various features which can be explained within the same framework (14; 15; 16). The main target we have been pursuing during the last year was to demonstrate the existence of state with macroscopic phase coherence in this compound.

The idea of BEC has already been used quite successfully to explain the transition of "normal" to "superfluid" $^4\mathrm{He}$. The strong interactions that exist in liquid $^4\mathrm{He}$ may alter the nature of the transition, however. For instance, while 90-95% of the particles of an atomic ensemble are in the "superfluid" phase below the transition temperature of an atomic BEC, just a few percent ($\sim$ 9%) of the Helium-atoms are condensed in superfluid $^4\mathrm{He}$.

One of the relevant parameters indicating that a system is Bose-Einstein condensed is the number of particles in the ground state N_c which gets macroscopically large for $T \to 0$K.

In the case of $\mathrm{TlCuCl_3}$ the total magnetization $M = g\mu_B N$ (17) is proportional to the total number of excited triplons N, where g is the Landé g-factor and μ_B is the Bohr magneton. We therefore analyzed this quantity in detail. The temperature dependence of the magnetization $M(T)$ along the applied magnetic field H shows a cusp-like minimum at a finite temperature $T_c(H)$ for fixed magnetic field H (see Fig. 11.6). The increase of M for $T < T_c$ is a consequence of the condensation of the magnetic quasiparticles and the increasing number of particles N_c in the ground state forming the condensate. Theoretical arguments predict a T-dependence of $M \propto \left(1 - \frac{T}{T_c}\right)^{\frac{3}{2}}$ (17).

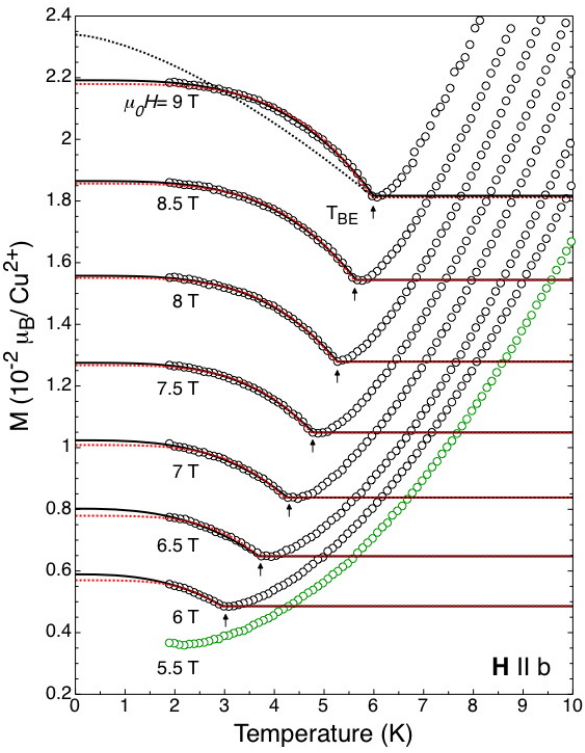

Figure 11.6: The total magnetization M per Cu^{2+} $TlCuCl_3$ for H ∥ b. The low-temperature regime for $T < T_c$ is fitted according to $g\mu_B n(T) = g\mu_B(n_{crit} + n_0(1 - (\frac{T}{T_c})^\alpha))$. The dashed red curves are for fixed α=4. The black curves are fits for varying exponent α. The black dotted curve represents a fit for $\alpha = \frac{3}{2}$ at $\mu_0 H$=9T.

We have fitted the low-temperature magnetization according to a more general power law

$$\begin{aligned} m(T) &= \frac{M(T)}{N_d} = g\mu_B \frac{N(T)}{N_d} = g\mu_B n(T) = \\ &= g\mu_B(n_{crit} + n_0\left(1 - \left(\frac{T}{T_c}\right)^\alpha\right)) \ , \end{aligned}$$

where N_d is the total number of dimers and $n_{crit} = \frac{N(T=T_c)}{N_d}$ is the critical density at which condensation occurs. This value corresponds to the normalized magnetization $m(T = T_c) = g\mu_B n_{crit}$. At zero temperature we obtain

$m(0) = g\mu_B n(0) = g\mu_B(n_{crit} + n_0)$ and therefore $n(0) = n_{crit} + n_0$. For an ideal Bose gas $n(0)$ corresponds to the condensate density. As soon as interactions between the particles are considered the depletion of the condensate has to be taken into account. The quantity $n(0) = n_c(0) + \tilde{n}(0)$ is then a sum of the condensate density $n_c(0)$ and the density of non-condensed particles $\tilde{n}(0)$. The latter term represents the number of triplons per Cu^{2+}-dimer scattered out of the ground state due the interactions between the particles. It depends on the number of condensed particles and can be expressed as $\tilde{n}(0) = \frac{1}{3\pi^2}\left(\frac{mUn_c(0)}{\hbar^2}\right)^{\frac{3}{2}}$, where $m \approx 2.8 \times 10^{-29}$ kg is the effective mass of a triplon and $\frac{U}{k_B} \approx 315\mathrm{K}$ (18) is the two-particle interaction potential . Extracting $n(0)$ from our fits, we can therefore calculate the condensate density at zero temperature $n_c(0)$ for various magnetic fields (see Fig. 11.7). As one would naively expect from simple arguments (17; 18) $n_c(0)$ increases with increasing magnetic field. The percentage of the condensed particles with respect to the total number of triplons is approximately 96% and slightly decreases with increasing magnetic field.

From this high percentage of condensed particles we conclude that the triplons in $\mathrm{TlCuCl_3}$ form a *weakly interacting Bose gas* right above H_c, and that the interaction increases with increasing particle density (i.e. with increasing the magnetic field H).

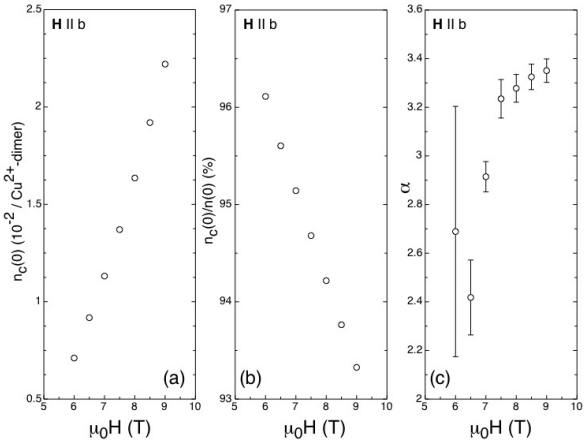

Figure 11.7:
(a) The number of condensed triplons per Cu^{2+} of $TlCuCl_3$ at T=0 K for H ‖ b.
(b) The percentage of particles in the condensate at T=0 K for H ‖ b.
(c) The extracted exponent α from $M(T < T_c)$ data of $TlCuCl_3$ for H ‖ b.

[1] H. Bartolf, *et al.*, accepted for publ. in Phys. C.

[2] A. Engel, *et al.*, submitted to J. Mod. Opt.

[3] C. P. Bean and J. D. Livingston, Phys. Rev. Lett., **12**, 14 (1964).

[4] A. Schilling and O. Jeandupeux; Phys. Rev. B; 52, 9714 (1995).

[5] A. Schilling and M. Reibelt; Rev. Sci. Instrum.; 78, 033904 (2007).

[6] K. A. Moler et al.; Phys. Rev. Lett.; 73, 2744 (1994).

[7] D. A. Wright et al.; Phys. Rev. Lett.; 82, 1550 (1999).

[8] G. E. Volovik; JETP Lett.; 58, 469 (1993).

[9] A. P. Ramirez et al.; Phys. Rev. Lett.; 74, 1218 (1995).

[10] C. Caroli and J. Matricon; Phys. Kondens. Mater.; 3, 380 (1965).

[11] A. P. Ramirez; Physics Letters A; 211, 59 (1996).

[12] M. Nohara et al.; Journal of the Physical Society of Japan; 66, 1888 (1997).

[13] G. M. Schmiedeshoff et al.; Phys. Rev. B; 63, 134519 (2001).

[14] B. Grenier et al., Phys. Rev. Lett. **92**, 087203 (2004).

[15] V. S. Zapf et al., Phys. Rev. Lett. **96**, 077204 (2006).

[16] M. Jaime et al., Phys. Rev. Lett. **93**, 077204 (2004).

[17] T. Nikuni et al., Phys.Rev. Lett. **84**, 5868 (2000).

[18] F. Yamada et al., condmat **arXiv:0711.2110v1** (2007).